

Article

Preparation and Properties of (YCa)(TiMn)O_{3-δ} Ceramics Interconnect of Solid Oxide Fuel Cells

Yi-Cheng Liou ^{1,2,*}, Wen-Chou Tsai ^{1,2}, Hao-Hsuan Yen ¹ and Yung-Chia Chang ¹

¹ Department of Electronic Engineering, Kun Shan University, No.195, Kunda Rd., Yongkang Dist., Tainan City 71070, Taiwan; E-Mails: wctsai@mail.ksu.edu.tw (W.-C.T.); s103001638@g.ksu.edu.tw (H.-H.Y.); a253591016@gmail.com (Y.-C.C.)

² Nano Technology R&D Center, Kun Shan University, No.195, Kunda Rd., Yongkang Dist., Tainan City 71070, Taiwan

* Author to whom correspondence should be addressed; E-Mail: ycliou@mail.ksu.edu.tw; Tel.: +886-6205-0521 (ext. 3706); Fax: +886-6205-0523.

Academic Editor: Teen-Hang Meen

Received: 7 June 2015 / Accepted: 6 July 2015 / Published: 10 July 2015

Abstract: (YCa)(TiMn)O_{3-δ} ceramics prepared using a reaction-sintering process were investigated. Without any calcination involved, the mixture of raw materials was pressed and sintered directly. Y₂Ti₂O₇ instead of YTiO₃ formed when a mixture of Y₂O₃ and TiO₂ with Y/Ti ratio 1/1 were sintered in air. Y₂Ti₂O₇, YTiO_{2.085} and some unknown phases were detected in Y_{0.6}Ca_{0.4}Ti_{0.6}Mn_{0.4}O_{3-δ}. Monophasic Y_{0.6}Ca_{0.4}Ti_{0.4}Mn_{0.6}O_{3-δ} ceramics were obtained after 1400–1500 °C sintering. Dense Y_{0.6}Ca_{0.4}Ti_{0.4}Mn_{0.6}O_{3-δ} with a density 4.69 g/cm³ was observed after 1500 °C/4 h sintering. Log σ for Y_{0.6}Ca_{0.4}Ti_{0.6}Mn_{0.4}O_{3-δ} increased from −3.73 Scm^{−1} at 350 °C to −2.14 Scm^{−1} at 700 °C. Log σ for Y_{0.6}Ca_{0.4}Ti_{0.4}Mn_{0.6}O_{3-δ} increased from −2.1 Scm^{−1} at 350 °C to −1.36 Scm^{−1} at 700 °C. Increasing Mn content decreased activation energy E_a and increased electrical conductivity. Reaction-sintering process is proved to be a simple and effective method to obtain (YCa)(TiMn)O_{3-δ} ceramics for interconnects in solid oxide fuel cells.

Keywords: (YCa)(TiMn)O_{3-δ}; interconnect; solid oxide fuel cells

1. Introduction

Solid oxide fuel cells (SOFCs) transform chemical energy from fuels, such as natural gas, humidified hydrogen, into electrical energy with high conversion efficiency and low pollution. An SOFC includes three principal components: the electrolyte, the cathode and the anode. Each part of the SOFC needs to be compatible both physically and chemically with one another to minimize interfacial reactions. A dense electrolyte is needed to prevent gas mixing, whereas the cathode and the anode must be porous to allow gas transport to the reaction sites. SOFCs generate electricity through the oxidation of fuel at anode and the reduction of oxygen at cathode. To provide a high voltage and power output, interconnects are used to connect the cells in series.

Lanthanum chromite (LaCrO_3) based perovskite oxides have been widely investigated as the ceramic interconnect for SOFCs due to their fairly high electrical conductivity and excellent thermodynamic stability at higher temperature [1,2]. $\text{La}_{0.7}\text{Ca}_{0.3}\text{Cr}_{0.5}\text{Co}_{0.5}\text{O}_3$ was reported with very high conductivity 85 Scm^{-1} at $700 \text{ }^\circ\text{C}$. However, its thermal expansion coefficient (TEC) increases from 11.12×10^{-6} to $19 \times 10^{-6} \text{ K}^{-1}$ due to the Co addition. This is much larger than acceptable values 11×10^{-6} – $12 \times 10^{-6} \text{ K}^{-1}$ for SOFC's design [1,3–5]. Dense LaCrO_3 based ceramics are not easy to prepare, besides, stoichiometric pellets are difficult to form because the high vapor pressure of constituent chromium at high temperature. To improve the sinterability of LaCrO_3 , some methods such as adding sintering aid, using a reducing atmosphere, and substituting lanthanum with other elements were tried by many researchers [6–12]. Chick *et al.* found $\text{La}_{0.7}\text{Ca}_x\text{CrO}_3$ with Ca deficiency, $x = 0.28$ and 0.29 , never attained 60% density, even at $1550 \text{ }^\circ\text{C}$ sintering. In contrast, the samples with Ca enrichment, $x = 0.31$ and 0.32 , attained densities over 90% at $1400 \text{ }^\circ\text{C}$ sintering [12]. Mori *et al.* reported $\text{La}_{0.8}\text{Sr}_{0.2}\text{CrO}_3$ having an average linear TEC of $9.9 \times 10^{-6} \text{ K}^{-1}$ in air and $12.2 \times 10^{-6} \text{ K}^{-1}$ in H_2 atmosphere, in the temperature range from 50 to $1000 \text{ }^\circ\text{C}$ [13]. Yang and co-workers investigated $\text{La}_{1-x}\text{Sr}_x\text{CrO}_3$ ($x = 0$ – 0.3) powder materials synthesized by the glycine-nitrate-process and found the maximum electrical conductivity 14.7 Scm^{-1} at $1000 \text{ }^\circ\text{C}$ in $\text{La}_{0.8}\text{Sr}_{0.2}\text{CrO}_3$ sintered at $1550 \text{ }^\circ\text{C}/2 \text{ h}$ [14]. Properties for LaCrO_3 based oxides have been improved when part of La is substituted by Ca or Sr.

Cr-free oxides were also investigated as interconnect for SOFCs. Taguchi *et al.* reported perovskite-type $(\text{La}_{0.1}\text{Ca}_{0.9})(\text{Mn}_{1-x}\text{Ti}_x)\text{O}_3$ ($0 \leq x \leq 0.9$) are n-type semiconductors at low temperature. At high temperature, the manganates exhibit a metal–insulator transition in the range $0 \leq x \leq 0.3$ [15]. Vashook *et al.* investigated perovskite-type compounds $\text{La}_{1-x}\text{Ca}_x\text{TiO}_3$ ($x = 0.2$ – 1.0) and $\text{La}_{2(1-x)/3}\text{Ca}_x\text{TiO}_3$ ($x = 0, 0.1, 0.4$ and 0.8). The crystal structures of the $\text{La}_{1-x}\text{Ca}_x\text{TiO}_3$ compounds at room temperature were as orthorhombic in space group Pbnm (samples with $0.7 \leq x \leq 1$) and as rhombohedral ($x = 0.6$). At room temperature three different perovskite-like structures has been found for A-deficient $\text{La}_{2(1-x)/3}\text{Ca}_x\text{TiO}_3$ compound: orthorhombic Pbnm structure for $x = 0.8$, orthorhombic Imma structure for $x = 0.4$, and monoclinic P2/m (or possibly orthorhombic Cm2m) structure for $x = 0.1$ [16]. Kobayashi *et al.* reported the crystal structures of $\text{Ca}_{0.5}\text{R}_{0.5}\text{Mn}_{0.5}\text{Ti}_{0.5}\text{O}_3$ ($\text{R} = \text{La}, \text{Nd}, \text{Eu}$) and $\text{Ca}_{0.67}\text{R}_{0.33}\text{Mn}_{0.33}\text{Ti}_{0.67}\text{O}_3$ ($\text{R} = \text{Y}, \text{Gd}, \text{Dy}, \text{Ho}, \text{Yb}$) are orthorhombic Pnma (No. 62) corresponding to GdFeO_3 type perovskite structure. The cell parameters b , c and cell volume increase with increasing ionic radius of rare earth element. The decrease in ionic radius of rare earth ions in these compounds makes increase distortion from ideal cubic perovskite [17]. Hosseini *et al.* fabricated lanthanum–manganese-doped CaTiO_3 perovskite oxides $\text{La}_{0.4}\text{Ca}_{0.6}\text{Ti}_{1-x}\text{Mn}_x\text{O}_{3-\delta}$ ($x = 0.0, 0.2, 0.4, 0.6$)

powders using an EDTA-citrate method and co-sintered as an interconnect material on an extruded porous anode substrate in a flat-tubular solid oxide fuel cell. The highest electrical conductivity occurs when $x = 0.6$; at 12.20 S cm^{-1} and 2.70 S cm^{-1} under oxidizing and reducing conditions [18]. Y^{3+} has typically been used to replace La^{3+} in ceramics containing lanthanum to improve their properties. We try to investigate the possibility of using $(\text{YCa})(\text{TiMn})\text{O}_{3-8}$ ceramics as interconnect for SOFCs.

In our previous studies, $\text{Pb}(\text{Mg}_{1/3}\text{Nb}_{2/3})\text{O}_3$ (PMN) and $\text{Pb}(\text{Fe}_{1/2}\text{Nb}_{1/2})\text{O}_3$ (PFN) ceramics had been prepared via a simple and effective reaction-sintering process [19,20]. Dense PMN ceramics (8.09 g/cm^3 , 99.5% of theoretic density 8.13 g/cm^3) with maximum dielectric constant 19,900 at 1 kHz were obtained. Other Pb-based complex perovskite ceramics were also successfully produced by this reaction-sintering process. In our recent investigations, some microwave dielectric ceramics such as BaTi_4O_9 , $\text{Ba}_5\text{Nb}_4\text{O}_{15}$, $\text{Sr}_5\text{Nb}_4\text{O}_{15}$, CaNb_2O_6 , NiNb_2O_6 , $\text{Zn}_{0.5}\text{Ti}_{0.5}\text{NbO}_4$ and $\text{Ni}_{0.5}\text{Ti}_{0.5}\text{NbO}_4$ were also prepared via this simple and effective reaction-sintering process [21–26]. In this study, preparation and properties of $(\text{YCa})(\text{TiMn})\text{O}_{3-8}$ ceramics via a reaction-sintering process were investigated.

2. Results and Discussion

The XRD profiles for the 2 h sintered YTiO_3 (YT), $\text{Y}_{0.6}\text{Ca}_{0.4}\text{Ti}_{0.6}\text{Mn}_{0.4}\text{O}_{3-8}$ (YCTM4) and $\text{Y}_{0.6}\text{Ca}_{0.4}\text{Ti}_{0.4}\text{Mn}_{0.6}\text{O}_{3-8}$ (YCTM6) ceramics are illustrated in Figure 1. The reflections for YT in Figure 1a match well with those of $\text{Y}_2\text{Ti}_2\text{O}_7$ (ICDD PDF # 00-042-0413) instead those of YTiO_3 (ICDD PDF # 00-027-1481). This implies that $\text{Y}_2\text{Ti}_2\text{O}_7$ formed more easily than YTiO_3 as the raw materials with Y/Ti ratio 1/1 were heated in air. Weak peaks (+) around 30° and 50.4° 2θ for $\text{YTiO}_{2.085}$ are seen in Figure 1a. Gill *et al.* prepared $\text{Y}_2\text{Ti}_2\text{O}_7$ from Y_2O_3 and Ti_2O_3 . After $800^\circ\text{C}/12 \text{ h}$ calcining, $\text{Y}_2\text{Ti}_2\text{O}_7$ phase along with weak $\text{YTiO}_{2.085}$ phase was detected for pellets sintered at $1500^\circ\text{C}/12 \text{ h}$. Almost monophasic $\text{YTiO}_{2.085}$ phase was detected for pellets sintered at $1550^\circ\text{C}/12 \text{ h}$ [27]. The reflections for YCTM4 in Figure 1b show that a phase with similar crystal structure of YTiO_3 formed as the major phase and $\text{Y}_2\text{Ti}_2\text{O}_7$ phase still formed in YCTM4. Weak peaks for $\text{YTiO}_{2.085}$ and some unknown phases are seen in Figure 1b. The reflections for major phase are also similar to those for $\text{Y}_{0.33}\text{Ca}_{0.67}\text{Ti}_{0.67}\text{Mn}_{0.33}\text{O}_3$ reported by Kobayashi *et al.* [17]. The crystal structure for YCTM4 is different from YT as Ca and Mn were added. The reflections for YCTM6 in Figure 1c show that only a phase with similar crystal structure of YTiO_3 and $\text{Y}_{0.33}\text{Ca}_{0.67}\text{Ti}_{0.67}\text{Mn}_{0.33}\text{O}_3$ reported by Kobayashi *et al.* [17] formed. $\text{Y}_2\text{Ti}_2\text{O}_7$ phase is not detected. More Mn addition inhibited the formation of $\text{Y}_2\text{Ti}_2\text{O}_7$, $\text{YTiO}_{2.085}$, and unknown phases. The reaction-sintering process is proved to be a simple and effective process to obtain YT, YCTM4 and YCTM6 ceramics. The calcination step of the conventional mixed oxide route was performed during the heating up period.

Relative density of YT, YCTM4 and YCTM6 ceramics sintered at various temperatures and soak time is shown in Figure 2. A low density, 69.1% of the theoretical density 4.98 g/cm^3 for $\text{Y}_2\text{Ti}_2\text{O}_7$, was found for $1400^\circ\text{C}/2 \text{ h}$ sintering YT pellets. Density of YT increased with sintering temperature and soak time. Dense YT with 91.4% of the theoretical density for $\text{Y}_2\text{Ti}_2\text{O}_7$ was observed after being sintered at $1500^\circ\text{C}/6 \text{ h}$. Gill *et al.* prepared $\text{Y}_2\text{Ti}_2\text{O}_7$ and obtained a low density 73% of the theoretical density after $800^\circ\text{C}/12 \text{ h}$ calcining and $1500^\circ\text{C}/12 \text{ h}$ sintering [27]. YCTM4 pellets show lower densities. YCTM4 with 77.9% of the theoretical density $\sim 4.97 \text{ g/cm}^3$ for $\text{Y}_{0.6}\text{Ca}_{0.4}\text{Ti}_{0.6}\text{Mn}_{0.4}\text{O}_{3-8}$ was observed even after sintering at $1500^\circ\text{C}/6 \text{ h}$. Lower densities may be caused by the unknown phases,

pores, and $\text{YTiO}_{2.085}$ with a low density 4.28 g/cm^3 . A higher sintering temperature or a prolonged sintering period is suggested for obtaining dense YCTM4. YCTM6 pellets show higher densities. Dense YCTM6 with 93.6% of the theoretical density $\sim 5.01 \text{ g/cm}^3$ for $\text{Y}_{0.6}\text{Ca}_{0.4}\text{Ti}_{0.4}\text{Mn}_{0.6}\text{O}_{3-\delta}$ was observed after being sintered at $1500 \text{ }^\circ\text{C}/4 \text{ h}$. The reaction-sintering process is proved to be effective at obtaining YT and YCTM6 ceramics with a relative density higher than 90%.

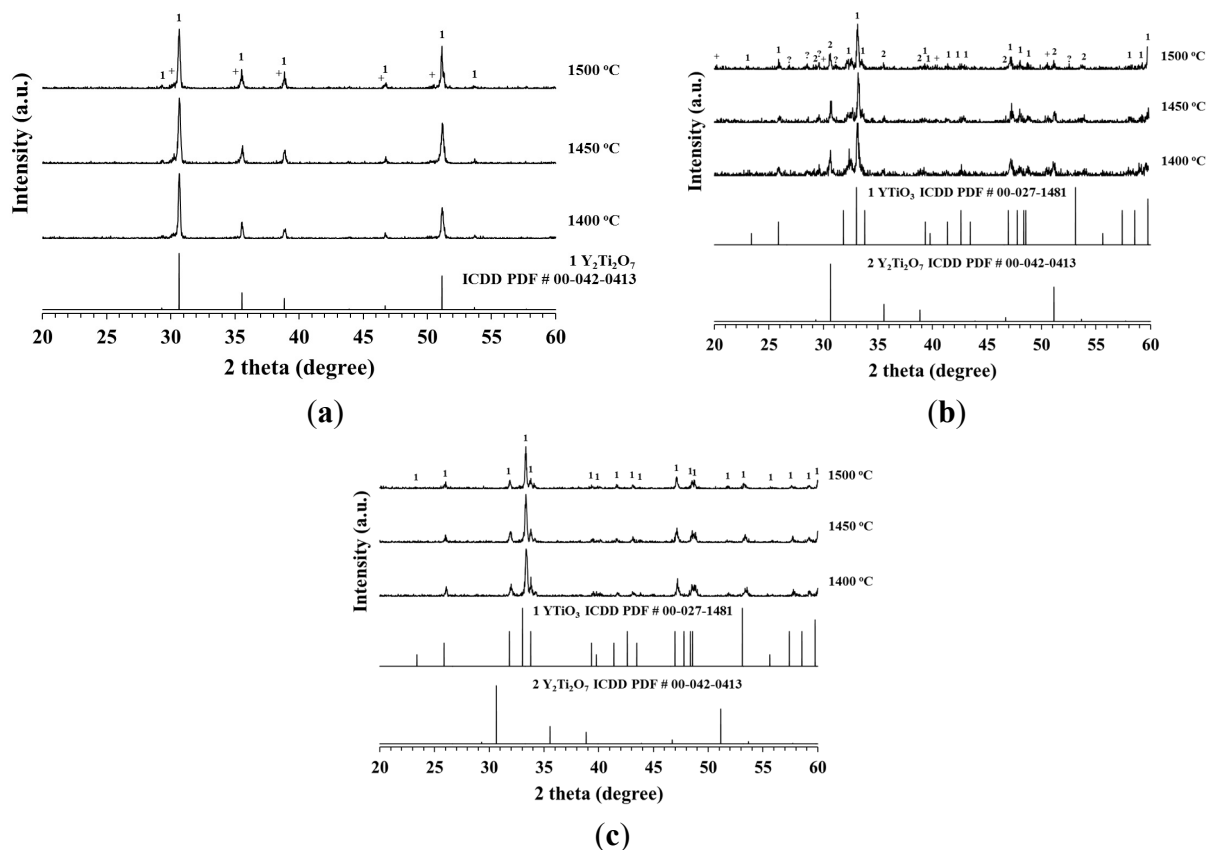


Figure 1. XRD patterns of the 2 h sintered (a) YTiO_3 (YT); (b) $\text{Y}_{0.6}\text{Ca}_{0.4}\text{Ti}_{0.6}\text{Mn}_{0.4}\text{O}_{3-\delta}$ (YCTM4); (c) $\text{Y}_{0.6}\text{Ca}_{0.4}\text{Ti}_{0.4}\text{Mn}_{0.6}\text{O}_{3-\delta}$ (YCTM6) ceramics. +: $\text{YTiO}_{2.085}$; ?: unknown phases.

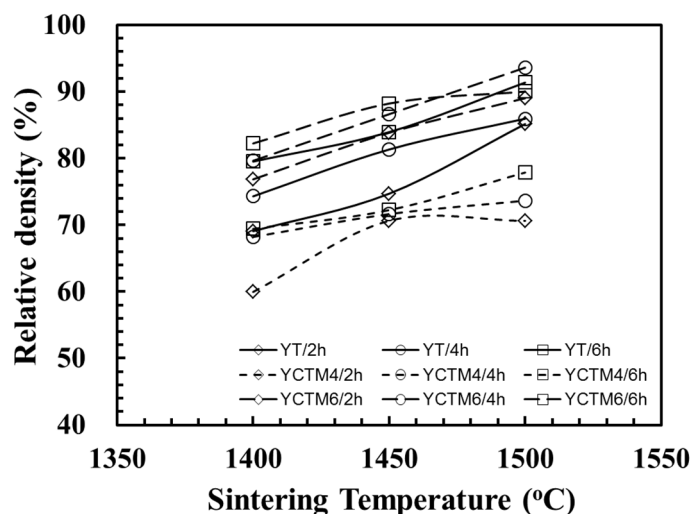


Figure 2. Relative density of YT, YCTM4, and YCTM6 ceramics sintered at various temperatures and soak time.

SEM photographs of as-fired YT ceramics sintered at various temperatures and soak time are presented in Figure 3. Porous pellets with grains smaller than 3 μm are seen for 1400 $^{\circ}\text{C}/2$ h sintering YT pellets. Grain size increased with sintering temperature and soak time. Grains > 10 μm are seen for 1500 $^{\circ}\text{C}/6$ h sintering YT pellets. Ding *et al.* prepared $\text{Y}_2\text{Ti}_2\text{O}_7$ with 1 mol% La_2O_3 and found grains smaller than 4 μm after 1450 $^{\circ}\text{C}/2$ –4 h sintering [28]. SEM photographs of the YCTM4 ceramics sintered at various temperatures and soak time are presented in Figure 4. Porous pellets with grains smaller than 8 μm are seen for 1400 $^{\circ}\text{C}/2$ h sintering YCTM4 pellets. Grain size increased with sintering temperature and soak time. Pores disappeared and grains >10 μm are seen for 1500 $^{\circ}\text{C}/6$ h sintering YCTM4 pellets. Grain growth increased as Ca and Mn were added into YT. Grains <4 μm are seen for $\text{La}_{0.4}\text{Ca}_{0.6}\text{Ti}_{0.6}\text{Mn}_{0.4}\text{O}_{3-\delta}$ via an EDTA-citrate method after 950 $^{\circ}\text{C}/5$ h calcining and 1400 $^{\circ}\text{C}/10$ h sintering [18]. Therefore, the reaction-sintering process is proved to be effective for grain growth in YT and YCTM4 ceramics. The calcinations stage and the following pulverization for the conventional solid-state reaction route could be bypassed. SEM photographs of the YCTM6 ceramics sintered at various temperatures and soak time are presented in Figure 5. Porous pellets with grains smaller than 6 μm are seen for 1400 $^{\circ}\text{C}/2$ h sintering YCTM6 pellets. Grain size increased with sintering temperature and soak time. Pores disappeared and grains > 20 μm are seen for 1500 $^{\circ}\text{C}/6$ h sintering YCTM6 pellets. More Mn addition increased the grain growth in YCTM6 pellets than in YCTM4 pellets. Grains <4 μm are seen for $\text{La}_{0.4}\text{Ca}_{0.6}\text{Ti}_{0.4}\text{Mn}_{0.6}\text{O}_{3-\delta}$ via an EDTA-citrate method after 950 $^{\circ}\text{C}/5$ h calcining and 1400 $^{\circ}\text{C}/10$ h sintering [18]. It is noted some cracks are seen in YCTM6 pellets. These cracks propagated not only along the grain boundaries but also through the grains. Besides, the amount and the size of cracks increased with sintering temperature and soak time. Sintering at temperatures below 1450 $^{\circ}\text{C}$ for a prolonged period or adding sintering aids are suggested for obtaining dense YCTM6 pellets without cracks.

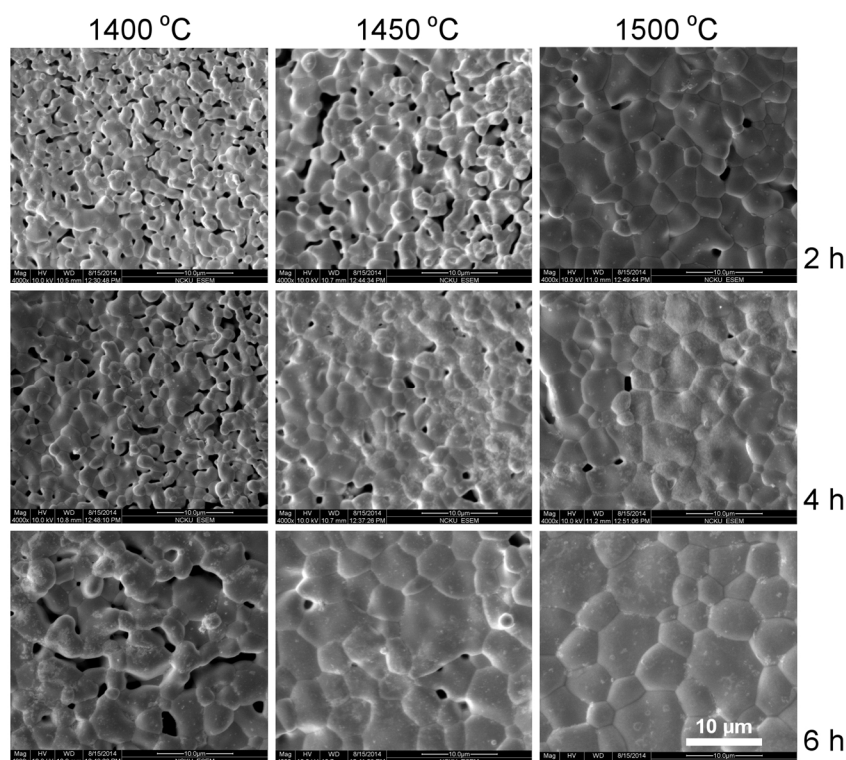


Figure 3. SEM photographs of the YT ceramics sintered at various temperatures and soak time.

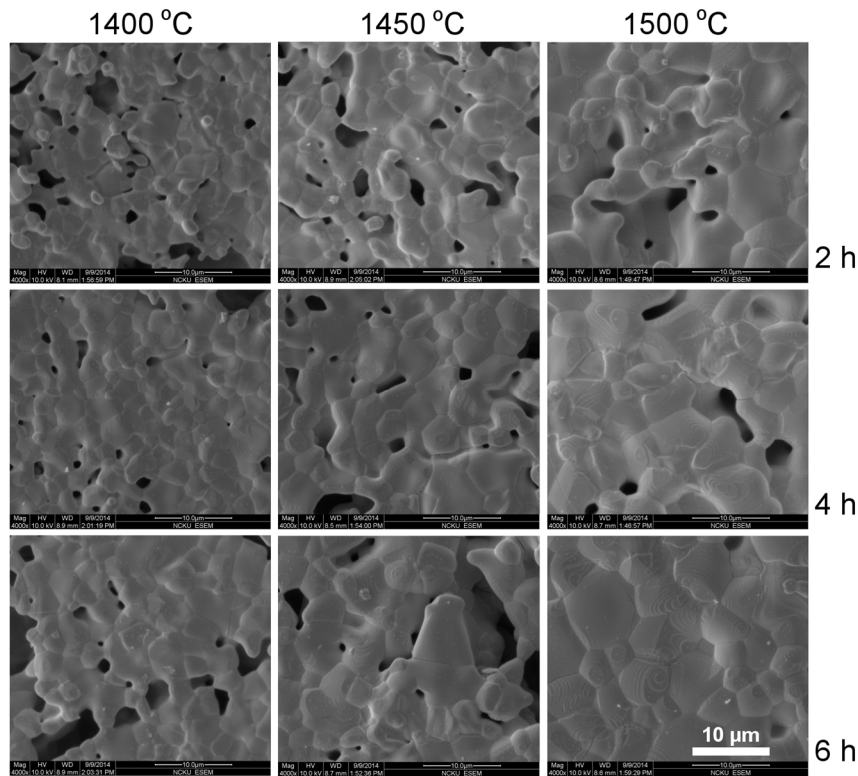


Figure 4. SEM photographs of the YCTM4 ceramics sintered at various temperatures and soak time.

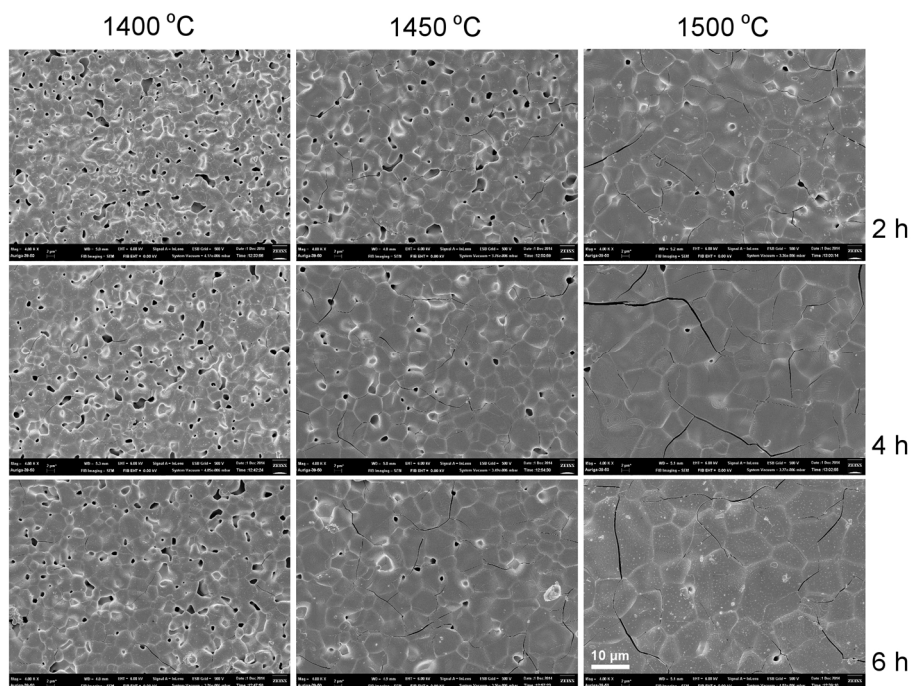


Figure 5. SEM photographs of the YCTM6 ceramics sintered at various temperatures and soak time.

DC total conductivity of 1500 °C/6 h sintering YT, YCTM4, and YCTM6 ceramics are shown in Figure 6. $\log \sigma$ is found from -8.19 Scm^{-1} at 350 °C to -4.94 Scm^{-1} at 700 °C for YT. Gill *et al.* prepared $\text{Y}_2\text{Ti}_2\text{O}_7$ and obtained $\log \sigma$ about -7.8 Scm^{-1} at 700 °C and -6.636 Scm^{-1} at 900 °C after 800 °C/12 h calcining and 1500 °C/12 h sintering [27]. The reaction-sintering process is proved to be effective at obtaining YT ceramics with a higher conductivity even the calcination was bypassed. $\log \sigma$ is

found from -3.73 Scm^{-1} at $350 \text{ }^\circ\text{C}$ to -2.14 Scm^{-1} at $700 \text{ }^\circ\text{C}$ for YCTM4. Conductivity increased as Ca and Mn were added into YT. σ about 1.5 Scm^{-1} at $700 \text{ }^\circ\text{C}$ for $\text{La}_{0.4}\text{Ca}_{0.6}\text{Ti}_{0.6}\text{Mn}_{0.4}\text{O}_{3-\delta}$ via an EDTA-citrate method after $950 \text{ }^\circ\text{C}/5 \text{ h}$ calcining and $1400 \text{ }^\circ\text{C}/10 \text{ h}$ sintering was obtained [18]. $\log \sigma$ is found from -2.1 Scm^{-1} at $350 \text{ }^\circ\text{C}$ to -1.36 Scm^{-1} at $700 \text{ }^\circ\text{C}$ for YCTM6. σ about 7 Scm^{-1} at $700 \text{ }^\circ\text{C}$ for $\text{La}_{0.4}\text{Ca}_{0.6}\text{Ti}_{0.4}\text{Mn}_{0.6}\text{O}_{3-\delta}$ via an EDTA-citrate method after $950 \text{ }^\circ\text{C}/5 \text{ h}$ calcining and $1400 \text{ }^\circ\text{C}/10 \text{ h}$ sintering was obtained [18]. Conductivity further increased as more Mn was added into YCTM4. A similar tendency was also observed in the study of $\text{La}_{0.4}\text{Ca}_{0.6}\text{Ti}_{1-x}\text{Mn}_x\text{O}_{3-\delta}$ by Hosseini *et al.* [18]. Conductivity increased as Mn content increased in $\text{La}_{0.4}\text{Ca}_{0.6}\text{Ti}_{1-x}\text{Mn}_x\text{O}_{3-\delta}$. According to the Arrhenius relationship [29], the experimental activation energy E_a can be determined from the slope of the line when natural logarithm of conductivity ($\ln \sigma$) is plotted against $1/T$ as shown in Figure 6. E_a for YT, YCTM4, and YCTM6 were derived as 1.18, 0.64, and 0.33 eV, respectively. E_a of 1.87 eV for $\text{La}_{0.4}\text{Ca}_{0.6}\text{TiO}_{3-\delta}$ and E_a of 0.47 eV for $\text{La}_{0.4}\text{Ca}_{0.6}\text{Ti}_{0.8}\text{Mn}_{0.2}\text{O}_{3-\delta}$ was obtained via an EDTA-citrate method after $950 \text{ }^\circ\text{C}/5 \text{ h}$ calcining and $1400 \text{ }^\circ\text{C}/10 \text{ h}$ sintering [18]. Hosseini *et al.* thought increasing Mn content decreased E_a and increased electrical conductivity in air. Increasing Mn content causes the number of oxygen vacancies to increase and this in turn causes an increase in electron hole concentration [18]. A similar tendency was also observed in this study.

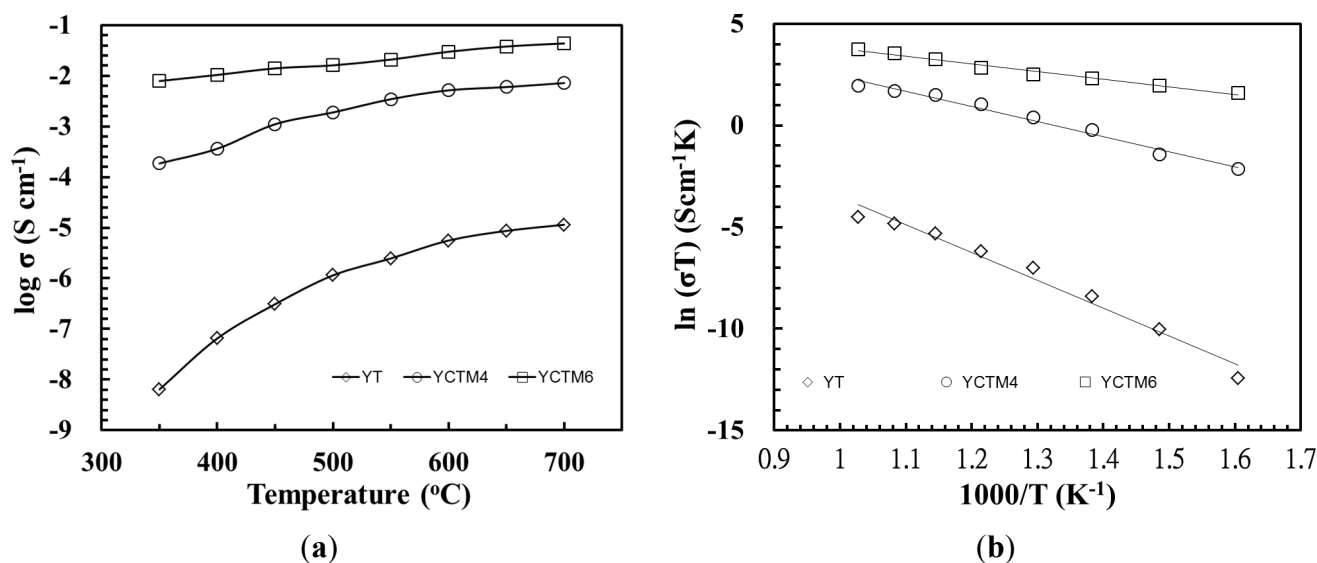


Figure 6. $\log \sigma$ and $\ln(\sigma T)$ of $1500 \text{ }^\circ\text{C}/6 \text{ h}$ sintering YT, YCTM4, and YCTM6 ceramics. (a) $\log \sigma$; (b) $\ln(\sigma T)$.

3. Experimental Section

YTiO_3 (YT), $\text{Y}_{0.6}\text{Ca}_{0.4}\text{Ti}_{0.6}\text{Mn}_{0.4}\text{O}_{3-\delta}$ (YCTM4) and $\text{Y}_{0.6}\text{Ca}_{0.4}\text{Ti}_{0.4}\text{Mn}_{0.6}\text{O}_{3-\delta}$ (YCTM6) samples in this study were prepared from reagent-grade powders: Y_2O_3 (99.9%, STREM CHEMICALS, Newburyport, MA, USA), CaCO_3 (99%, SHOWA, Tokyo, Japan), TiO_2 (99.9%, SHOWA, Tokyo, Japan), and MnO_2 (99.9%, J.T. Baker, Phillipsburg, NJ, USA). Appropriate amounts of raw materials for each batch were weighed and put into a PE (Polyethylene) bottle. Zirconia balls with 5 and 10 mm diameters were used for milling the raw mother powders with de-ionized water for 12 h at a speed of 500 rpm. The dried and pulverized powders were pressed into pellets with 12 mm in diameter and 1–2 mm thick. The pellets were sintered at $1400\text{--}1500 \text{ }^\circ\text{C}$ at a rate $10 \text{ }^\circ\text{C}/\text{min}$ in a covered alumina crucible in air.

The reflections of various phases for the sintered pellets were analyzed by XRD. Microstructures were analyzed by scanning electron microscopy (SEM). The density of the sintered pellets was measured using the Archimedes method. Ag electrodes were formed on both sides of the sintered pellets. Agilent 34970A Data Acquisition was used for electrical resistivity measurements at 350–700 °C.

4. Conclusions

(YCa)(TiMn)O_{3-δ} ceramics could be effectively obtained via a simple reaction-sintering process with the calcining stage bypassed. Y₂Ti₂O₇ instead of YTiO₃ formed when a mixture of Y₂O₃ and TiO₂ with Y/Ti ratio 1/1 were heated in air. Y₂Ti₂O₇, YTiO_{2.085} and some unknown phases were detected in Y_{0.6}Ca_{0.4}Ti_{0.6}Mn_{0.4}O_{3-δ}. Monophasic Y_{0.6}Ca_{0.4}Ti_{0.4}Mn_{0.6}O_{3-δ} ceramics were obtained after 1400–1500 °C sintering. Y_{0.6}Ca_{0.4}Ti_{0.6}Mn_{0.4}O_{3-δ} with a density 3.87 g/cm³ was observed even at 1500 °C/6 h sintering. Dense Y_{0.6}Ca_{0.4}Ti_{0.4}Mn_{0.6}O_{3-δ} with a density 4.69 g/cm³ was observed after 1500 °C/4 h sintering. Some cracks are seen in Y_{0.6}Ca_{0.4}Ti_{0.4}Mn_{0.6}O_{3-δ} pellets. Log σ is found from −3.73 Scm^{−1} at 350 °C to −2.14 Scm^{−1} at 700 °C for Y_{0.6}Ca_{0.4}Ti_{0.6}Mn_{0.4}O_{3-δ}. Log σ is found from −2.1 Scm^{−1} at 350 °C to −1.36 Scm^{−1} at 700 °C for Y_{0.6}Ca_{0.4}Ti_{0.4}Mn_{0.6}O_{3-δ}. Increasing Mn content decreased activation energy E_a and increased electrical conductivity. Reaction-sintering process is proved to be a simple and effective method for obtaining (YCa)(TiMn)O_{3-δ} ceramics for interconnects in solid oxide fuel cells.

Author Contributions

Yi-Cheng Liou formulated research ideas and wrote initial manuscript. Analysis of data was performed by Yi-Cheng Liou and Wen-Chou Tsai. Hao-Hsuan Yen and Yung-Chia Chang performed the experiments. All authors read and approved the manuscript.

Conflicts of Interest

The authors declare no conflict of interest.

References

1. Fergus, J.W. Lanthanum chromite-based materials for solid oxide fuel cell interconnects. *Sol. State Ion.* **2004**, *171*, 1–15.
2. Sakai, N.; Kawada, T.; Yokokawa, H.; Dokiya, M. Sinterability and electrical conductivity of calcium-doped lanthanum chromites. *J. Mater. Sci.* **1990**, *25*, 4531–4534.
3. Tao, S.W.; Irvine, J.T.S. A redox-stable efficient anode for solid-oxide fuel cells. *Nat. Mater.* **2003**, *2*, 320–323.
4. Zhu, W.Z.; Deevi, S.C. Development of interconnect materials for solid oxide fuel cells. *Mater. Sci. Eng. A* **2003**, *348*, 227–243.
5. Sakai, N.; Yokokawa, H.; Horita, T.; Yamaji, K. Lanthanum chromite-based interconnects as key materials for SOFC stack development. *Int. J. Appl. Ceram. Tech.* **2004**, *1*, 23–30.
6. Group, L.; Anderson, H.U. Densification of La_{1-x}Si_xCrO₃. *J. Am. Ceram. Soc.* **1976**, *59*, 449–450.
7. Sakai, N.; Kawada, T.; Yokokawa, H.; Dokiya, M.; Kojima, I. Liquid-phase-assisted sintering of calcium-doped lanthanum chromites. *J. Am. Ceram. Soc.* **1993**, *76*, 609–616.

8. Hayashi, S.; Fukaya, K.; Saito, H. Sintering of lanthanum chromite doped with zinc or copper. *J. Mater. Sci. Lett.* **1988**, *7*, 457–458.
9. Bansal, K.P.; Kumari, S.; Das, B.K.; Jain, G.C. Electrical conduction in titania-doped lanthanum chromite ceramics. *J. Mater. Sci.* **1981**, *16*, 1994–1998.
10. Sammes, N.M.; Ratnaraj, R.; Fee, M.G. The effect of sintering on the mechanical properties of SOFC ceramic interconnect materials. *J. Mater. Sci.* **1994**, *29*, 4319–4324.
11. Wang, J.; Ponton, C.B.; Marquis, P.M. Sintering and microstructural development of $\text{La}_{0.80}\text{Ca}_{0.22}\text{CrO}_3$. *J. Mater. Sci. Lett.* **1996**, *15*, 658–661.
12. Chick, L.A.; Liu, J.; Stevenson, J.W.; Armstrong, T.R.; McCready, D.E.; Maupin, G.D.; Coffey, G.W.; Coyle, C.A. Phase transitions and transient liquid-phase sintering in calcium-substituted lanthanum chromite. *J. Am. Ceram. Soc.* **1997**, *80*, 2109–2120.
13. Mori, M.; Yamamoto, T.; Itoh, H.; Watanabe, T. Compatibility of alkaline earth metal (Mg, Ca, Sr)-doped lanthanum chromites as separators in planar-type high-temperature solid oxide fuel cells. *J. Mater. Sci.* **1997**, *32*, 2423–2431.
14. Yang, Y.J.; Wen, T.L.; Tu, H.; Wang, D.Q.; Yang, J. Characteristics of lanthanum strontium chromite prepared by glycine nitrate process. *Sol. State Ion.* **2000**, *135*, 475–479.
15. Taguchi, H.; Sonoda, M.; Nagao, M.; Kido, H. Role of tetravalent ion in metal–insulator transition in $(\text{La}_{0.1}\text{Ca}_{0.9})(\text{Mn}_{1-x}\text{Ti}_x)\text{O}_3$. *J. Sol. State Chem.* **1996**, *126*, 235–241.
16. Vashook, V.; Vasylechko, L.; Knapp, M.; Ullmann, H.; Guth, U. Lanthanum doped calcium titanates: Synthesis, crystal structure, thermal expansion and transport properties. *J. Alloy. Compd.* **2003**, *354*, 13–23.
17. Kobayashi, M.; Katsuraya, R.; Kurita, S.; Yamaguchi, M.; Satoh, H.; Kamegashira, N. Synthesis and crystal structure of $(\text{Ca},\text{R})(\text{Mn},\text{Ti})\text{O}_3$ (R, rare earth). *J. Alloy. Compd.* **2006**, *408–412*, 1173–1176.
18. Hosseini, N.R.; Sammes, N.M.; Chung, J.S. Manganese-doped lanthanum calcium titanate as an interconnect for flat-tubular solid oxide fuel cells. *J. Power Sour.* **2014**, *245*, 599–608.
19. Liou, Y.C.; Tseng, K.H. Stoichiometric $\text{Pb}(\text{Mg}_{1/3}\text{Nb}_{2/3})\text{O}_3$ perovskite ceramics produced by reaction-sintering process. *Mater. Res. Bull.* **2003**, *38*, 1351–1357.
20. Liou, Y.C.; Shih, C.Y.; Yu, C.H. Stoichiometric $\text{Pb}(\text{Fe}_{1/2}\text{Nb}_{1/2})\text{O}_3$ perovskite ceramics produced by reaction-sintering process. *Mater. Lett.* **2003**, *57*, 1977–1981.
21. Liou, Y.C.; Wu, C.T.; Tseng, K.H.; Chung, T.C. Synthesis of BaTi_4O_9 ceramics by reaction-sintering process. *Mater. Res. Bull.* **2005**, *40*, 1483–1489.
22. Liou, Y.C.; Shiue, W.H.; Shih, C.Y. Microwave ceramics $\text{Ba}_5\text{Nb}_4\text{O}_{15}$ and $\text{Sr}_5\text{Nb}_4\text{O}_{15}$ prepared by a reaction-sintering process. *Mater. Sci. Eng. B* **2006**, *131*, 142–146.
23. Liou, Y.C.; Weng, M.H.; Shiue, C.Y. CaNb_2O_6 ceramics prepared by a reaction-sintering process. *Mater. Sci. Eng. B* **2006**, *131*, 14–19.
24. Liou, Y.C.; Shiue, C.Y.; Weng, M.H. Synthesis and properties of TiO_2 added NiNb_2O_6 microwave dielectric ceramics using a simple process. *J. Eur. Ceram. Soc.* **2009**, *29*, 1165–1171.
25. Chen, Y.T.; Liou, Y.C.; Fung, K.Z. $(1-x)\text{ZnNb}_2\text{O}_6-x\text{TiO}_2$ microwave dielectric ceramics by reaction-sintering process. In Proceedings of the 2007 MRS-T annual meeting, Hsinchu, Taiwan, 16–17 November 2007. (In Chinese)

26. Chen, Y.T.; Liou, Y.C.; Fung, K.Z. $\text{Ni}_{0.5}\text{Ti}_{0.5}\text{NbO}_4$ microwave ceramics by a reaction-sintering process. In Proceedings of the 2007 MRS-T annual meeting, Hsinchu, Taiwan, 16–17 November 2007. (In Chinese)
27. Gill, J.K.; Pandey, O.P.; Singh, K. Role of sintering temperature on thermal, electrical and structural properties of $\text{Y}_2\text{Ti}_2\text{O}_7$ pyrochlores. *Int. J. Hydrog. Energy* **2011**, *36*, 14943–14947.
28. Ding, J.; Xiao, Y.; Han, P.; Zhang, Q. Effects of rare earth oxides on dielectric properties of $\text{Y}_2\text{Ti}_2\text{O}_7$ series ceramics. *J. Rare Earths* **2010**, *28*, 765–768.
29. Moulson, A.J.; Herbert, J.M. *Electroceramics: Materials, Properties, Applications*, 2nd ed.; John Wiley & Sons Ltd: Chichester, UK, 2003; p. 32.

© 2015 by the authors; licensee MDPI, Basel, Switzerland. This article is an open access article distributed under the terms and conditions of the Creative Commons Attribution license (<http://creativecommons.org/licenses/by/4.0/>).